












RESEARCH ARTICLE

Upregulation of the secretory pathway $\text{Ca}^{2+}/\text{Mn}^{2+}$ -ATPase isoform 1 in LPS-stimulated microglia and its involvement in Mn^{2+} -induced Golgi fragmentation

Aysha M. Bhojwani-Cabrera¹  | Alicia Bautista-García¹  |
Veronika E. Neubrand¹  | Francisco A. Membrive-Jiménez¹  | Mattia Bramini¹  |
David Martin-Oliva¹  | Miguel A. Cuadros¹  | José Luis Marín-Teva¹  |
Julio Navascués¹  | Peter Vangheluwe²  | M. Rosario Sepúlveda¹ 

¹Department of Cell Biology, Faculty of Sciences, University of Granada, Granada, Spain

²Laboratory of Cellular Transport Systems, Department of Cellular and Molecular Medicine, KU Leuven, Leuven, Belgium

Correspondence

M. Rosario Sepúlveda, Department of Cell Biology, Faculty of Sciences, University of Granada. Avda. Fuentenueva s/n, Granada 18151, Spain.
Email: mrsepulveda@ugr.es

Funding information

FEDER-Junta de Andalucía, Grant/Award Number: A1-CTS-324-UGR18; UGR Research Program, Grant/Award Number: PP2022. PP.29

Abstract

Microglia play an important protective role in the healthy nervous tissue, being able to react to a variety of stimuli that induce different intracellular cascades for specific tasks. Ca^{2+} signaling can modulate these pathways, and we recently reported that microglial functions depend on the endoplasmic reticulum as a Ca^{2+} store, which involves the Ca^{2+} transporter SERCA2b. Here, we investigated whether microglial functions may also rely on the Golgi, another intracellular Ca^{2+} store that depends on the secretory pathway $\text{Ca}^{2+}/\text{Mn}^{2+}$ -transport ATPase isoform 1 (SPCA1). We found upregulation of SPCA1 upon lipopolysaccharide stimulation of microglia BV2 cells and primary microglia, where alterations of the Golgi ribbon were also observed. Silencing and overexpression experiments revealed that SPCA1 affects cell morphology, Golgi apparatus integrity, and phagocytic functions. Since SPCA1 is also an efficient Mn^{2+} transporter and considering that Mn^{2+} excess causes manganism in the brain, we addressed the role of microglial SPCA1 in Mn^{2+} toxicity. Our results revealed a clear effect of Mn^{2+} excess on the viability and morphology of microglia. Subcellular analysis showed Golgi fragmentation and subsequent alteration of SPCA1 distribution from early stages of toxicity. Removal of Mn^{2+} by washing improved the culture viability, although it did not effectively reverse Golgi fragmentation. Interestingly, pretreatment with curcumin maintained microglia cultures viable, prevented Mn^{2+} -induced Golgi fragmentation, and preserved SPCA Ca^{2+} -dependent activity, suggesting curcumin as a potential protective agent against Mn^{2+} -induced Golgi alterations in microglia.

KEYWORDS

brain, calcium, Golgi, manganese, manganism, microglia, secretory pathway

This is an open access article under the terms of the [Creative Commons Attribution](https://creativecommons.org/licenses/by/4.0/) License, which permits use, distribution and reproduction in any medium, provided the original work is properly cited.

© 2024 The Authors. GLIA published by Wiley Periodicals LLC.

1 | INTRODUCTION

Microglia are highly dynamic cells that are continuously surveying neural tissue. They constitute the resident immune cells in the brain and are reactive to many different stimuli that lead to microglial migration, proliferation, release of specific cytokines, or phagocytosis (Sierra et al., 2019). Thus, microglia can act in a protective and anti-inflammatory manner in brain injury and against toxins or infections, although a contribution to pro-inflammatory events underlying different neuropathologies has also been described (Tang & Le, 2016; Ton et al., 2002; Wolf et al., 2017). Ca^{2+} signaling is emerging as a key mechanism that determines the microglial phenotype that ranges from neuroprotective to pro-inflammatory. Many of the microglial triggers lead to Ca^{2+} oscillations (Hoffmann et al., 2003), since a precise and controlled increase in cytosolic Ca^{2+} concentrations ($[\text{Ca}^{2+}]_c$) is the first step of a signaling cascade that regulates the expression of genes required to modulate the aforementioned microglial functions. Later, the recovery of basal $[\text{Ca}^{2+}]_c$ is necessary to respond to new signals or to prevent cellular damage after overstimulation. Nevertheless, not all the molecular players involved in Ca^{2+} homeostasis in microglia have yet been identified.

The dynamic nature of microglia also requires a sophisticated endomembrane system to perform their characteristic morphological changes and functions. Thus, a well-developed endoplasmic reticulum (ER), Golgi apparatus and secretory pathway, as well as other endomembrane compartments, are present in these cells. The luminal Ca^{2+} concentration in these organelles is critical to perform their intrinsic functions, but also serves as Ca^{2+} stores that participate in Ca^{2+} signaling processes across the cell. In this sense, we recently reported the upregulation of the ER Ca^{2+} -ATPase (SERCA2b) after lipopolysaccharide (LPS)-stimulation of microglia in culture and in amoeboid microglia in brains of Alzheimer's disease patients (Morales-Ropero et al., 2021). Inhibition of SERCA2b in microglia caused opposite effects on migration and phagocytosis, highlighting the crucial role of these Ca^{2+} -transporters and the ER Ca^{2+} store in mechanisms that modulate microglia in health and disease.

To determine whether other intracellular Ca^{2+} stores and transporters may also be involved, we decided to focus our attention on the secretory pathway Ca^{2+} -ATPase (SPCA), a primary active Ca^{2+} transporter that was the last one to be identified in the nervous system. Like SERCA2b, SPCA also belongs to the P-type ATPase family but while SERCA2b transports 2 Ca^{2+} ions per ATP into the ER, SPCA only pumps 1 Ca^{2+} ion into the trans-Golgi or secretory pathway per molecule of ATP (reviewed in Chen et al. (2020)). There are two genes ATP2C1 and ATP2C2 that encode two isoforms, SPCA1 and SPCA2, with SPCA1 representing the ubiquitous isoform highly expressed in brain (Sepulveda et al., 2008; Sepulveda et al., 2009), whereas SPCA2 presents a much more restricted distribution, especially in exocrine glands (Feng & Rao, 2013; Vanoevelen et al., 2005). In contrast to other Ca^{2+} pumps, SPCA can also transport Mn^{2+} with high affinity (Ton et al., 2002). Mn^{2+} overexposure is associated to an occupational disease called manganism, which shares many symptoms with Parkinson's disease (Aschner et al., 2009; Racette et al., 2012); however,

specific Mn^{2+} transporters in the nervous system have not been identified yet. Interestingly, Mn^{2+} accumulation occurs in brain regions with high SPCA1 expression (Sepulveda, Dresselaers, et al., 2012), and elevated doses of Mn^{2+} affect Ca^{2+} -dependent SPCA activity and Golgi integrity in cultured neurons and astrocytes (Sepulveda, Wuytack, & Mata, 2012). However, the role of SPCA1 in microglia and Mn^{2+} toxicity has not been explored so far.

Thus, in this work, we studied for the first time the expression, localization, and function of SPCA1 in microglial cells, particularly challenged with LPS that triggers an inflammatory response of microglia. Additionally, we analyzed the involvement of the Golgi apparatus and the SPCA1 transporter during Mn^{2+} overexposure in microglia.

2 | MATERIALS AND METHODS

2.1 | BV2-microglial cell line and primary culture from mouse brain microglia

BV2 cells were cultured in RPMI medium containing 10% (v/v) fetal bovine serum (GIBCO), 2 mM L-glutamine, 100 U/mL penicillin, and 100 $\mu\text{g}/\text{mL}$ streptomycin; and were incubated at 37°C in a humidified environment of 5% CO_2 .

Primary cultures of mouse brain microglia were prepared from newborn (1 or 2-days old) C57BL/6 mice as previously described (Neubrand et al., 2018) with modifications (Morales-Ropero et al., 2021). Animals were obtained from the Animal Facility Service of the Scientific Instrument Centre of the University of Granada (UGR), and experiments were performed with the approval from the UGR Ethical Committee. Cells were stimulated with 100 ng/mL bacterial LPS (serotype 0111:B4, Sigma).

2.2 | Immunocytochemistry and fluorescence microscopy

BV2 cells or primary microglia (25,000 cells) were seeded onto 12 mm (diameter) round glass coverslips coated with 0.1 mg/mL poly-D-lysine. After treatment, cells were fixed with cold 4% paraformaldehyde in PBS for 20 min. Then, cells were permeabilized with 0.2% (v/v) Triton X-100 in PBS and blocked with 3% bovine serum albumin (BSA) in PBS for 1 h. Subcellular co-localization of proteins was determined by incubation with the corresponding primary antibody for 2 h: polyclonal rabbit anti-SPCA1 (1:500, [Van Baelen et al., 2001]) and monoclonal mouse anti-GM130 (1:250, BD Biosciences). Fluorescence labeling was obtained by the corresponding secondary antibodies Alexa594 goat anti-rabbit and Alexa488 goat anti-mouse (1:2000, Thermo Fisher). The actin cytoskeleton was stained with phalloidin-FITC (1:50, Sigma), and DAPI was used for nuclei staining. Images were taken with the Zeiss Axiophot fluorescent microscope. To verify that curcumin was inside the cells, orthogonal projections were obtained with a Leica TCS SP5 confocal microscopy.

2.3 | Transmission electron microscopy

Primary microglia were cultured in 6-well plates coated with 0.1 mg/mL poly-D-lysine (250,000 cells/well). After the corresponding treatment, cells were washed with cold PBS and fixed with 1.5% glutaraldehyde, 1% formaldehyde in 0.05 M cacodylate buffer (pH 7.4) supplemented with 2 mM MgCl₂, and 0.03 g/L saccharose for 2 h, postfixed in 1% osmium tetroxide for 1 h, stained with 2% uranyl acetate for 2 h, dehydrated in graded series of ethanol, and embedded in Embed812 resin. Ultrathin sections (50–70 nm) were obtained in an ultramicrotome Reichert Jung, mounted on copper grids, and stained by double contrast with uranyl acetate and lead citrate. Images were taken with a Zeiss Libra 120 EDX electron microscope.

2.4 | Cell analysis

Images were analyzed by Image J software (version 1.50i, NIH). The cell morphology was characterized by analysis of the aspect ratio of individual cells according to Alawieyah Syed Mortadza et al. (2018), where higher values than 1.0 indicate enhanced cell ramification and elongation, or cell surface area. Quantification of immunostaining intensities was determined in terms of Integrated Density (the product of Area and Mean Gray Value). Golgi fragmentation determined by fluorescence microscopy was defined as “fragmentation” when Golgi stacks were not compacted in a Golgi ribbon, but they were found dispersed throughout the cytoplasm.

2.5 | Preparation of protein extracts

Cells were seeded at a density of 1.5×10^6 cell per p10 plate or 200,000 cells per well in 6-well plates. After treatment, cells were harvested by scraping and pelleting. Protein extracts were prepared using 50-mM Tris/HCl pH 8.0, 0.1-mM EDTA, 0.5% Triton X-100 and 12.5 mM β -mercaptoethanol as lysis buffer, and vortexing every 5 min for 45 min on ice. After centrifugation at $16,000 \times g$ for 15 min, protein extracts were obtained in the supernatant. Alternatively, membrane fractions were prepared following the protocol described by Sepulveda et al. (2005). Protein concentration was measured with the Bio-Rad Protein Assay using BSA as standard.

2.6 | Western blotting

Twenty micrograms of protein extracts were electrophoresed in 7.5% (w/v) SDS-polyacrylamide gels and transferred to polyvinylidene difluoride membranes using a Trans-Blot SD semidry system (Bio-Rad). After blocking in Tris-buffered saline (TBS) containing 5% (w/v) of non-fat dry milk and 0.3% Tween 20 for 1 h, immunostaining reactions were performed by incubating the membranes for 3 h at room temperature with the following primary antibodies

diluted in TBS-1% (v/v) Tween 20: anti-SPCA1 (1:1000), and anti β -tubulin (1:3000, Sigma). Afterwards, membranes were incubated for 1 h at room temperature with peroxidase-conjugated secondary antibodies (1:5000, Bio-Rad) and revealed with Immobilon Western substrate (Millipore) using the ChemiDoc-It (UVP) and VisionWorks LS software.

2.7 | SPCA ATPase activity

A coupled enzymatic assay was used in specific conditions to measure the SPCA-dependent Ca²⁺-ATPase activity in membrane fractions, by adding 100-nM thapsigargin and 2- μ M vanadate to inhibit SERCA and plasma membrane Ca²⁺-ATPase activities, respectively, as described in Sepulveda et al. (2008).

2.8 | DNA transfection

BV2 cells seeded on coated glass coverslips at a density of 25,000 cells were transfected with 1 μ g of the plasmids iSPCA1-pSUPER for silencing or SPCA1-pEGFP for overexpression using the GenJuice transfection reagent (Merck). In the silencing assay, cells were co-transfected with an empty plasmid that express the green fluorescent protein (GFP) at 10:1, so that it can be assumed that GFP-positive cells were also transfected successfully with iSPCA1-pSUPER. Cells were analyzed after incubation for 72 h at 37°C in a humidified environment of 5% CO₂.

2.9 | Cell viability

Cell viability was determined using the 3-[4,5-dimethylthiazol-2-yl]-2,5-diphenyl tetrazolium bromide (MTT) method. Briefly, cells were seeded in 96-well culture plates (30,000 cells per well). After treatment, the cells were incubated with 1 mg/mL MTT for 3 h at 37°C. Metabolically active cells reduced MTT to a formazan precipitate that was solubilized with DMSO and quantified spectrophotometrically at 595 nm in a microplate spectrophotometer reader (Multiskan Ascent, Thermo Scientific).

2.10 | Phagocytosis assays

Fluorescent red-latex beads (mean particle diameter 1 μ m, Sigma) were pre-opsonized in 50% FBS in sterile PBS for 1 h and loaded to transfected BV2 cells seeded in coverslips at concentration of 50 beads per cell for 4 h at 37°C. Subsequently, cells were extensively washed to remove remaining beads, fixed in 4% paraformaldehyde in PBS for 20 min at room temperature, and mounted on glass slides with FluorSave mounting medium. Images were captured with the Zeiss Axiophot fluorescent microscope and quantification of phagocytosis from GFP-positive cells was performed.

2.11 | Data processing and statistical analysis

Data were processed and analyzed with the SigmaPlot v10 software and significant differences were determined by unpaired Student's *t*-test or by one-way ANOVA with Duncan multiple range tests for multiple comparisons by using IBM SPSS Statistics v20. Statistical significance was assumed at $p \leq .05$.

3 | RESULTS

3.1 | SPCA1 is upregulated in LPS-stimulated microglia

We used primary microglia from newborn mouse brain and the bacterial endotoxin LPS to analyze the inflammatory phenotype of microglia (Figure 1). Phalloidin staining showed the characteristic change in morphology from homeostatic microglia with small cellular body and long processes to LPS-stimulated microglia with a more amoeboid morphology (Figure 1a). Morphological analysis showed a significant reduction of the aspect ratio parameter after LPS activation, corresponding to a more rounded shape (Figure 1b). Then, we analyzed the expression and subcellular localization of the SPCA1 by immunocytochemistry (Figure 1c, d). Control cells showed the expected subcellular localization of SPCA1 mainly in the perinuclear region, where the Golgi complex is localized, as observed with the cis-Golgi marker GM130. When microglial cells were incubated with LPS, a small but significant increase in the integrated density corresponding to the Golgi-localized SPCA1 was found (Figure 1d). A similar SPCA1 distribution was observed in control and LPS-stimulated BV2 cells (Figure S1), a microglial cell line with similar characteristics as primary cultured microglia (Henn et al., 2009). Further analysis by transmission electron microscopy in control primary microglial cultures showed a Golgi ribbon with 7–10 stacks in close proximity to the perinuclear area, while LPS-stimulated cells exhibited dilated cisternae with groups of stacks retained to the perinuclear area and other stacks with a more disperse distribution (Figure 1e). The distances from each Golgi stack to the nucleus or between proximal Golgi stacks (Figure 1f) were significantly different. The distance from Golgi stacks to the nucleus in control cells was $2.37 \pm 0.22 \mu\text{m}$, while the distance in LPS-stimulated cells was $1.09 \pm 0.19 \mu\text{m}$ for the perinuclear Golgi stacks and $5.93 \pm 0.40 \mu\text{m}$ for the dispersed group. The distance between proximal Golgi stacks was 0.99 ± 0.06 or $1.81 \pm 0.62 \mu\text{m}$ in control or LPS conditions, respectively.

Next, SPCA1 protein expression in microglial extracts was analyzed by Western blotting (Figure 2). The specific SPCA1 antibody recognized two distinct and closely spaced SPCA1-positive bands around 100 kDa. The lower protein band migrated at the same molecular weight as the band immunodetected in mouse brain extracts. Both SPCA1-positive bands found in primary microglia were 1.5 times upregulated after LPS stimulation (Figure 2b). Similar results were obtained in BV2 microglial cells (Figure 2a,b). Additionally, SPCA-mediated Ca^{2+} -ATPase activity was similarly increased in LPS-stimulated primary microglia and BV2 cells (Figure 2c).

3.2 | Silencing and overexpression of SPCA1 alter morphology, Golgi integrity, and phagocytosis efficiency in BV2 cells

We carried out transient transfections of BV2-cells with the plasmid iSPCA1-pSUPER for SPCA1 silencing and SPCA1-pEGFP for SPCA1 overexpression (Figure 3). The SPCA1 protein levels were quantified by Western blotting (Figure 3a), showing a significant reduction or increase of SPCA1 after silencing or overexpression, respectively. No effect on cell viability was observed after silencing or overexpression compared with control cells transfected with the empty plasmids pSUPER or pEGFP (Figure 3b). Immunocytochemistry and fluorescence microscopy with anti-SPCA1 antibodies revealed SPCA1 localization at the juxtannuclear area in control cells, while almost no immunoreaction was detected after SPCA1 silencing confirming the specificity of the SPCA1 antibody signal (Figure 3c). Following overexpression, the SPCA1 distribution was altered to small Golgi stacks dispersed through the cytoplasm. In both SPCA1-silenced and SPCA1-overexpressing cells, the cell morphology shifted to a rounded shape, which was quantified as a significant decrease in the aspect ratio parameter (Figure 3d). A significant reduction of cell area was observed in SPCA1-overexpressing cells (Figure 3d). To analyze the involvement of SPCA1 in microglial functions, we used fluorescent red-latex beads to determine the phagocytic capacity (Figure 3e). Silencing of SPCA1 impaired phagocytosis in microglia, while SPCA1 overexpression induced a slight increase in the number of phagocytosed particles.

3.3 | Manganese overexposure affects cell viability and SPCA activity, and causes Golgi fragmentation in microglia

SPCA differs from other Ca^{2+} pumps because it can also transport Mn^{2+} with high affinity. Thus, we investigated the effect of Mn^{2+} overexposure on microglial cells. Figure 4a shows that incubations with increasing Mn^{2+} concentrations drastically reduced cell viability of both BV2 and primary microglia cultures with similar IC_{50} values (2.5 mM MnCl_2 at 6 h). The toxicity was more pronounced at longer exposure time (IC_{50} of 1 mM MnCl_2 at 24 h).

We also analyzed cell morphology of primary microglia (Figure 4b) and BV2 cells (Figure S2A) at low Mn^{2+} concentrations. Cells exhibited a rather rounded morphology with process retraction compared with controls. Since SPCA1 is a trans-Golgi located protein, we studied Golgi integrity by double immunostaining with the cis-Golgi marker anti-GM130 and the anti-SPCA1 antibodies in primary microglia (Figure 4c) and BV2 cells (Figure S2B). A fragmented Golgi staining dispersed throughout the cytoplasm (arrowheads) was observed from low Mn^{2+} concentrations, being more evident in the trans-Golgi than in the cis-Golgi compartment. No pyknotic nuclei with condensed chromatin were observed in the cultures after DAPI staining (Figure 4c), suggesting that Golgi fragmentation represents an early event, which takes place before other characteristic signs of cellular damage in microglia. The quantification of cells with unfragmented or

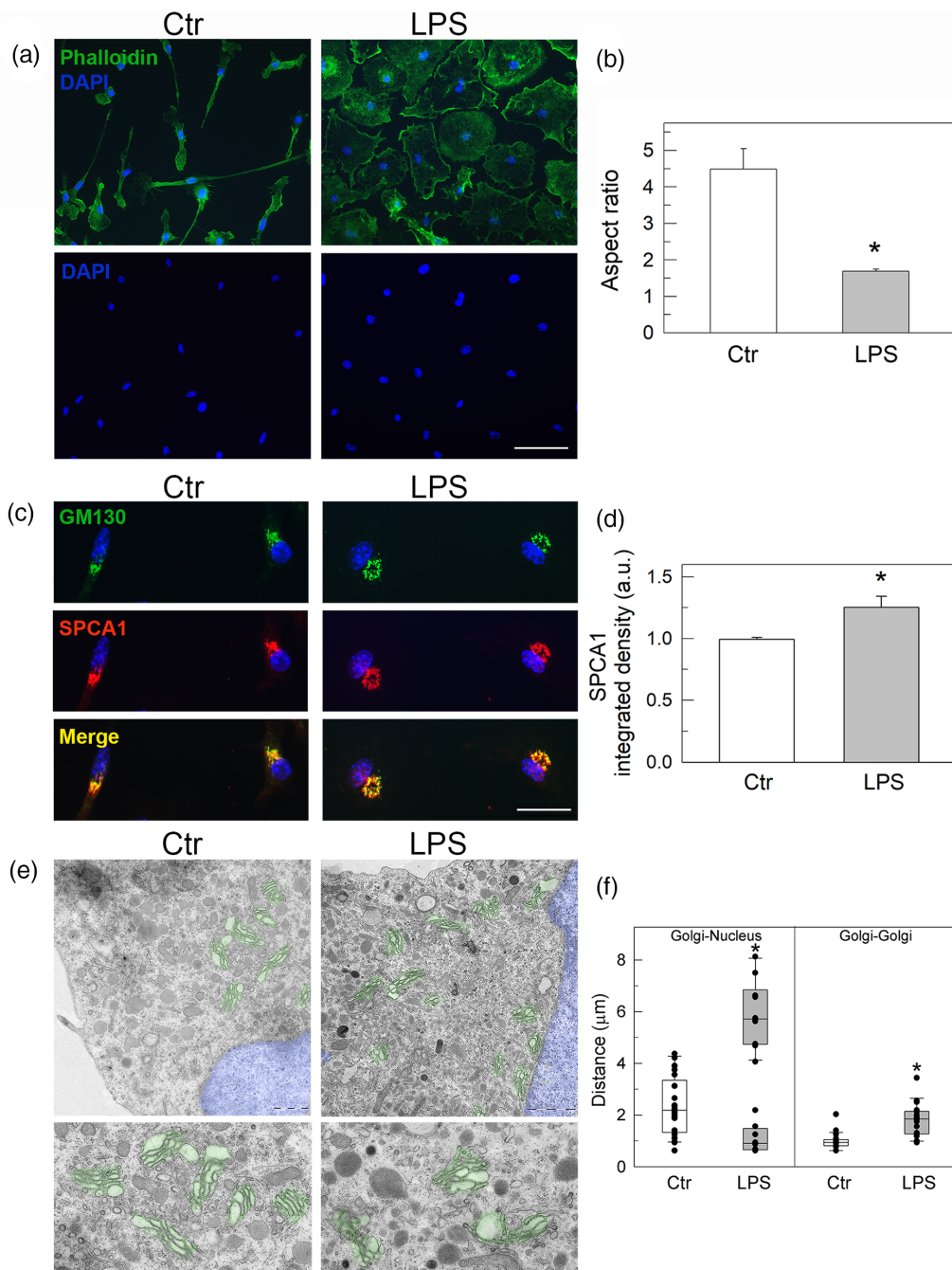


FIGURE 1 Subcellular distribution of SPCA1 and Golgi apparatus morphology in control and LPS-stimulated primary microglia from mouse brain. (a) Phalloidin staining (green) to visualize actin cytoskeleton showed the expected change in morphology from control microglia in culture with small cellular bodies and long processes (Ctr) to LPS-stimulated microglia with amoeboid morphology (LPS). Cell nuclei were visualized by DAPI staining (blue), showing similar cell densities (lower panel). (b) Morphological analysis showed a reduction of the aspect ratio in LPS-stimulated cells, corresponding to rounder cells compared with controls. (c) Immunocytochemistry with the cis-Golgi marker GM130 (green) and the SPCA1 (red) antibodies at the same cell density as Figure 1c. The higher magnification shows a co-localization at the juxtannuclear Golgi (Merge) in control and LPS-stimulated microglia. (d) Integrated density of SPCA1 immunostaining showing a slight, but significantly higher value in the presence of LPS compared with the control. Data collected from three independent experiments, analyzing at least 40 cells per condition in each experiment. (e) Analysis of the Golgi apparatus by transmission electron microscopy showing Golgi stacks (pseudo-colored in green) in close proximity to the nucleus (in blue) in control microglia, while dilated cisternae and dispersed stacks were observed under LPS conditions. (f) Quantification of distance from Golgi stacks to the nucleus and between Golgi stacks. Control primary microglial cultures (Ctr) showed Golgi ribbons with 7–10 stacks in close proximity to the perinuclear area, while LPS-stimulated cells (LPS) exhibited dilated cisternae with groups of stacks retained to the perinuclear area (lower gray box plot) and other stacks with a more dispersed distribution, and thus, larger distance from the Golgi stacks to the nucleus (upper gray box plot). At least five cells per condition were analyzed, counting at least seven Golgi stacks per cell. Data are mean \pm SEM (*, $p < .05$). Scale bars: 20 μ m (a); 10 μ m (c); 1 μ m (e). LPS, lipopolysaccharide; SPCA1, secretory pathway Ca²⁺/Mn²⁺-transport ATPase isoform 1.

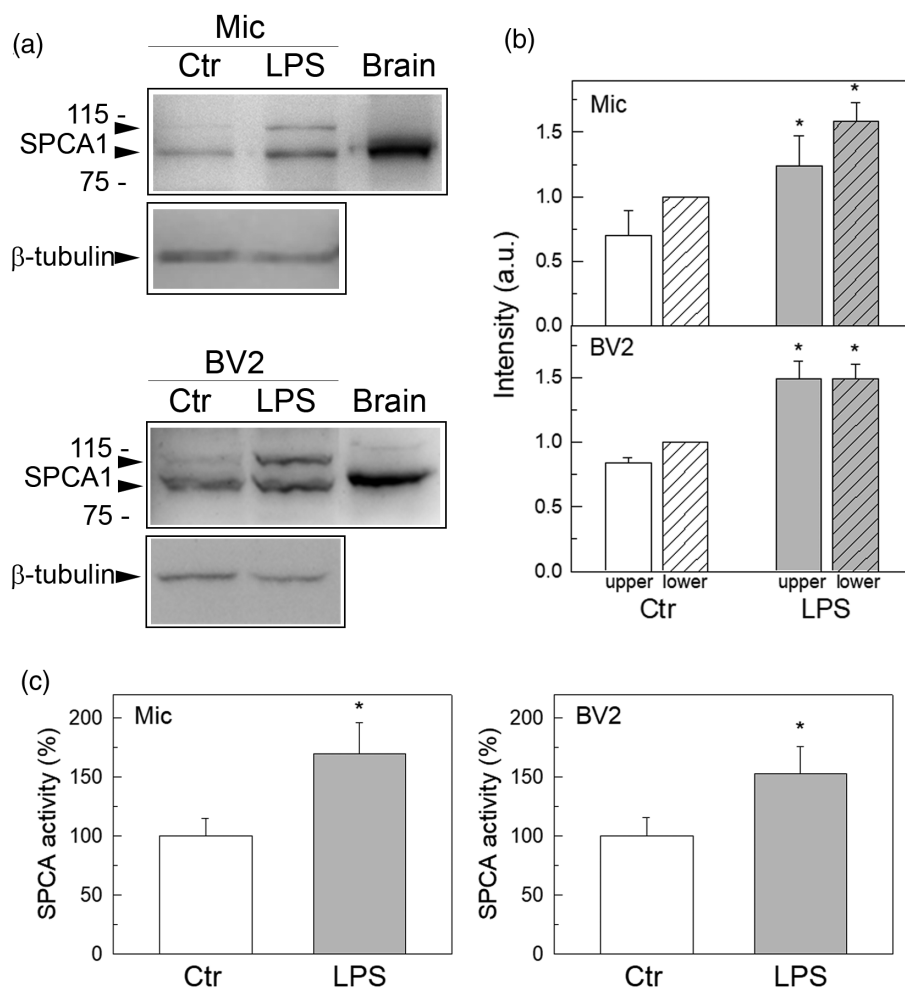


FIGURE 2 SPCA1 expression in control and LPS-stimulated microglia. (a) Representative Western blots using the anti-SPCA1 antibody in protein extracts from primary microglia from mouse brain (Mic) and from the BV2 cell line (BV2) in control (Ctr) and LPS (LPS) conditions. Molecular weight markers are indicated on the left. Adult mouse brain (Brain) was used as control for the SPCA1 immunoreaction and β -tubulin as loading control. (b) Quantification of intensities of SPCA1 upper (non-stripped bars) and lower (striped bars) bands normalized to the loading control β -tubulin, in controls (white bars) and LPS-stimulated (gray bars) cells. They were normalized to the SPCA1 lower band in controls (value of 1.0 arbitrary units) in both primary and BV2 microglia. (c) SPCA Ca²⁺-ATPase activity in control and LPS-stimulated primary microglia and BV2 cells. 100% activity corresponds to 0.025 ± 0.003 and $0.063 \pm 0.01 \mu\text{mol min}^{-1} \text{mg}^{-1}$ for primary microglia and BV2 cells, respectively. Data are means \pm SEM of three experiments performed in duplicates (*, $p < .05$). LPS, lipopolysaccharide; SPCA1, secretory pathway Ca²⁺/Mn²⁺-transport ATPase isoform 1.

fragmented Golgi revealed that 50% of cells exhibited fragmentation after 6-h incubation with 1 mM MnCl₂ for BV2 cells (Figure 4d) or 0.5 mM MnCl₂ for primary microglia (Figure 4e), concentrations that corresponded to 80% and 90% of cell viability, respectively (Figure 4a).

We further studied if SPCA1 protein expression levels changed during the Mn²⁺-elicited Golgi fragmentation by Western blot (Figure 5). No significant changes in the SPCA1 protein were observed in BV2 cells and primary microglia from cultures treated with 0.1 and 0.5 mM MnCl₂ for 6 h (Figure 5a,b), which had shown high Golgi fragmentation in the previous experiment (Figure 4). However, the SPCA-dependent Ca²⁺-ATPase activity was reduced in BV2-membrane vesicles after incubation with MnCl₂ (Figure 5c), suggesting that high Mn²⁺ concentrations may interfere with SPCA Ca²⁺ transport in the cell affecting Ca²⁺ dynamics. To investigate the direct involvement of SPCA1 function in Mn²⁺ toxicity, we altered SPCA1 expression by silencing and overexpression and subsequent overexposure of cells to Mn²⁺ (Figure 5d), showing a decrease or an increase in cell viability, respectively.

As it is known that manganese symptoms can be reduced after cessation of the Mn²⁺ overexposure (Avila et al., 2013; Benedetto et al., 2009), we tested if microglial cells could recover from the MnCl₂-induced toxicity by withdrawal. To address this, cells were first

exposed to 1 or 2.5 mM MnCl₂ for 6 h. Subsequently, the culture medium was fully replaced by medium from parallel untreated cultures, and cells were analyzed after 24 h (Figure 6). The washout halted the progression of Mn²⁺-induced cytotoxicity in BV2 cells in terms of cell viability (Figure 6a) and Golgi fragmentation (Figure 6b). However, primary microglia were more sensitive to the replacement of the medium than BV2 cells, even when no manganese treatment was applied (Figure 6c,d). In addition, the washout was insufficient to stop the manganese-induced cytotoxic effect in primary cultures at these concentrations and recovery time points.

3.4 | Curcumin pretreatment prevents Mn²⁺-induced toxicity in microglia

Curcumin exhibits antioxidant and anti-inflammatory properties and presents special biological properties following complexation with metals (Shakeri et al., 2019). Thus, the effect of curcumin against Mn²⁺-induced toxicity in microglial cultures was analyzed. Figure 7a,b shows that curcumin uptake by primary microglia can be visualized due to its fluorescence when excited at wavelengths close to 500 nm. Pre-incubation with 10- μ M curcumin 1 h before Mn²⁺ exposure induced a

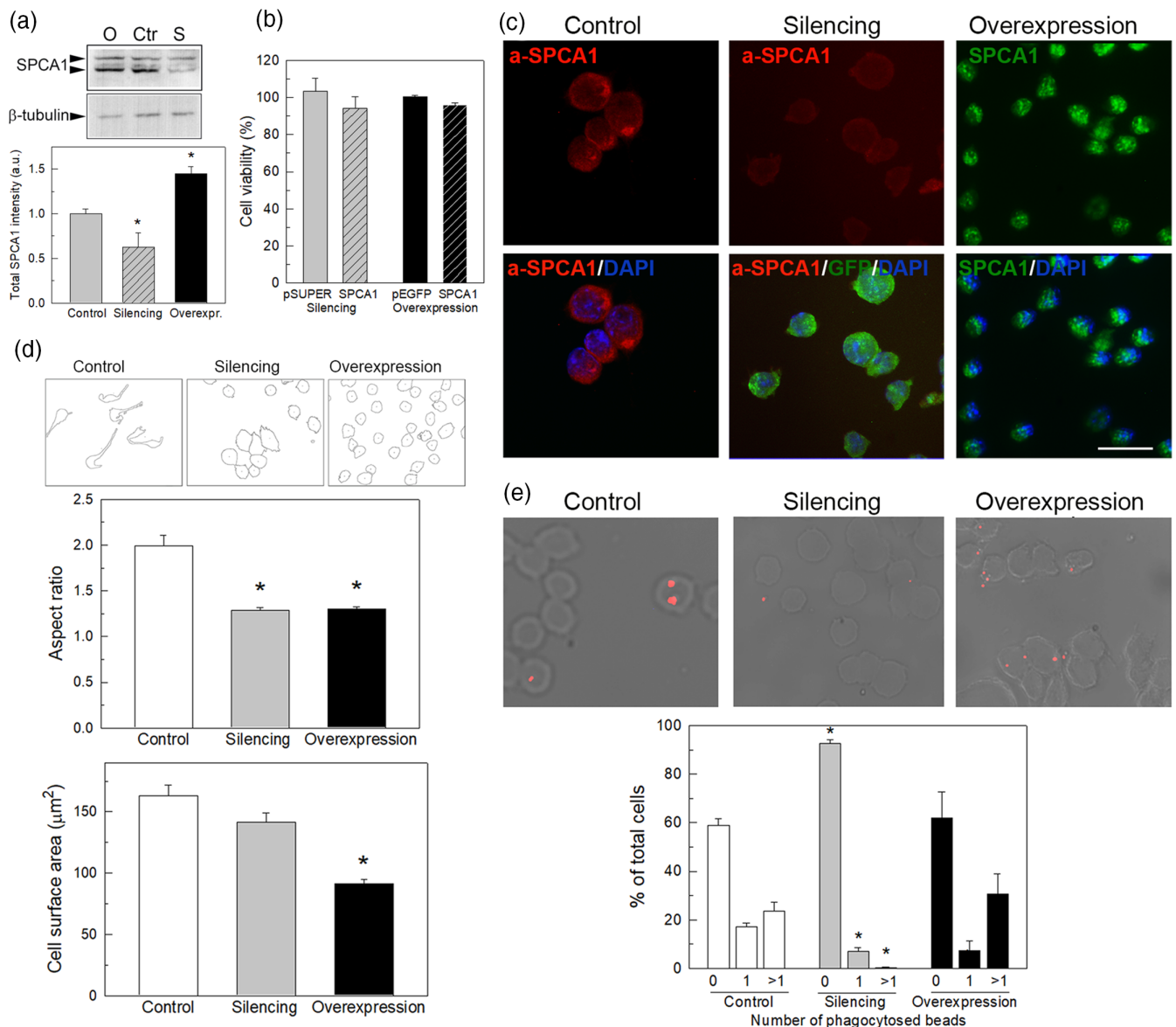


FIGURE 3 Effects of SPCA1 silencing and over-expression on BV2 microglial cells. (a) Representative Western blot using the anti-SPCA1 antibody in protein extracts from BV2 cells after transfections. Quantification of total SPCA1 intensities normalized to the loading control β -tubulin, in controls, SPCA1-silenced and SPCA1-overexpressing cells. (b) Effects of SPCA1 silencing and overexpression on BV2 cell viability. MTT assays showed no significant effect on cell viability after transfection with empty plasmids (pSUPER, pEGFP), or iSPCA1-pSUPER and SPCA1-pEGFP for silencing and overexpression, respectively. (c) Localization and expression of SPCA1 in transfected cells. Immunostaining with the anti-SPCA1 antibody determined its localization to the Golgi apparatus (red) in control cells. This staining is almost absent in GFP-positive silenced cells (green). Overexpressed SPCA1-GFP appeared to be distributed in small spots throughout the cytoplasm suggesting Golgi fragmentation. DAPI staining (blue) was used to visualize nuclei. (d) Analysis of cell morphology in images obtained by phase-contrast microscopy. Upper panel shows representative outlines used to analyze morphological parameters. A significant reduction of the aspect ratio is observed in transfected cells corresponding to a more amoeboid morphology in contrast to the characteristics branched control cells. Determination of cell area showed a significant reduction in SPCA1-overexpressing cells. (e) Phagocytosis assays in the three conditions using fluorescent latex beads. Representative bright-field images merged with red fluorescent phagocytosed latex beads are shown. Quantification of the phagocytosis assay is shown in the lower panel. The percentage of cells that engulf 0, 1, or more than 1 particle is significantly different in SPCA1-silenced cells. Data are mean \pm SEM of three experiments, analyzing at least 40 cells per condition in each experiment. (*, $p < .01$) compared with control. Scale bars: 20 μm (c, e). SPCA1, secretory pathway $\text{Ca}^{2+}/\text{Mn}^{2+}$ -transport ATPase isoform 1.

protective effect on cell viability to Mn^{2+} -induced toxicity, while post-treatment with curcumin after 6-h Mn^{2+} incubation did not halt the toxicity (Figure 7c). We further observed a significant reduction of Golgi fragmentation in curcumin-pretreatment experiments (Figure 7d,e).

Similar results were obtained in BV2 cells (data not shown). In addition, the SPCA-dependent Ca^{2+} -ATPase activity was protected from Mn^{2+} inhibition by curcumin (Figure 7f), and the effects of curcumin were not modulated by SPCA1 expression levels (Figure 7g).

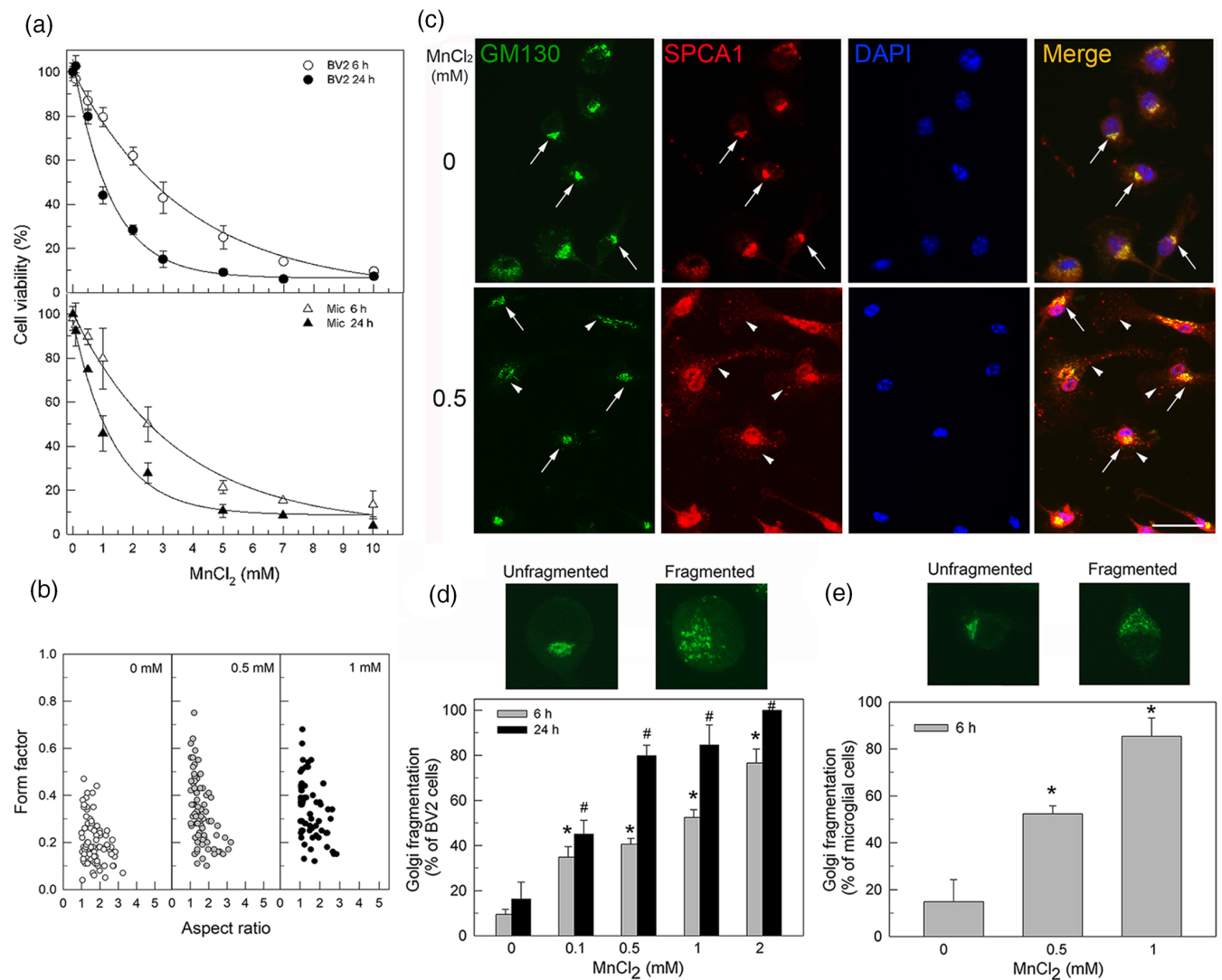


FIGURE 4 Effect of manganese on cell viability and Golgi integrity of microglia. (a) Cell viability of BV2 cells (BV2) and primary microglia (Mic) after exposure to increasing concentrations of MnCl₂ for 6 or 24 h. (b) Scatterplot including the morphological parameters form factor and aspect ratio, showing a shift towards a higher number of amoeboid primary microglia after Mn²⁺ exposure. (c) Double immunofluorescence with the cis-Golgi marker GM130 (green) and the anti-SPCA1 (red) antibodies in primary microglia exposed to 0 and 0.5 mM MnCl₂ for 6 h. DAPI staining (blue) was used to visualize nuclei. Cells exhibited compact Golgi (arrows) or fragmented Golgi scattered throughout the cytoplasm (arrowheads) at low Mn²⁺ concentrations when cell viability was barely affected. (d, e) Representative images of GM130 immunoreactions showing unfragmented and fragmented Golgi used for the quantification in BV2 cells (d) and primary microglia (e). Data are mean ± SEM of four experiments in duplicates. To quantify the form factor or Golgi fragmentation, we analyzed at least 30 cells per condition in each experiment. *p* < .05 compared with the control without MnCl₂-treatment at 6 h (*) or 24 h (#). Scale bar in (c): 20 μm. SPCA1, secretory pathway Ca²⁺/Mn²⁺-transport ATPase isoform 1.

To further analyze the Mn²⁺ effect on Golgi ribbon integrity in primary microglia, we used transmission electron microscopy (Figure 8). Mn²⁺ exposure induced Golgi fragmentation into small mini-stacks that appeared to maintain the cis-medial-trans structure but with shorter cisternae, and an increase in Golgi-derived vesicles. These Golgi mini-stacks were more dispersed in the cytoplasm, compared with the perinuclear and compact localization of the Golgi apparatus shown by control cells. As observed in the immunofluorescence assays, curcumin pretreatment significantly preserved Golgi integrity from Mn²⁺-induced fragmentation.

4 | DISCUSSION

In this work, we have analyzed the protein expression and subcellular localization of the trans-Golgi Ca²⁺/Mn²⁺-ATPase SPCA1 in untreated and LPS-treated microglia. Our results are in agreement with available gene expression databases, showing high levels of Atp2c1 transcripts in microglia, which are increased after LPS stimulation (Friedman et al., 2018). Via toll-like receptor 4 (TLR4), LPS triggers Ca²⁺ influx increasing [Ca²⁺]_i, and subsequently, Ca²⁺ storage. This is consistent with the upregulation of the intracellular Ca²⁺

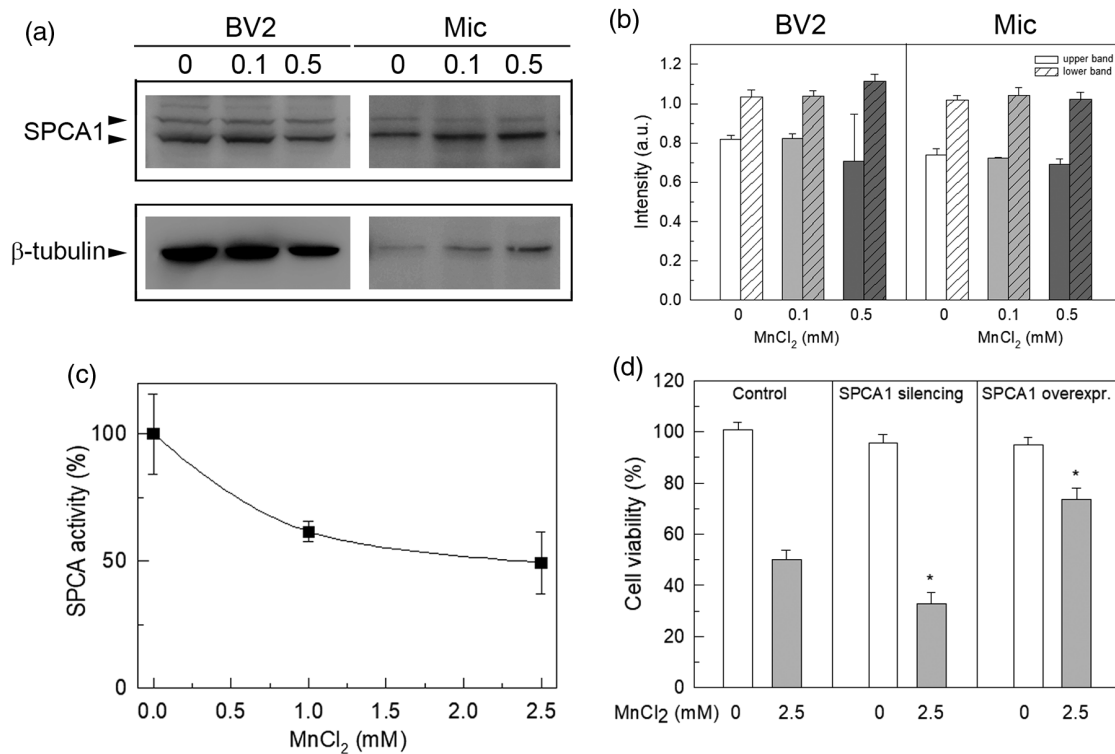


FIGURE 5 Effect of Mn^{2+} on protein expression and activity of SPCA from BV2 and primary microglia cultures. (a) Representative Western blots using the anti-SPCA1 antibody in protein extracts from BV2 cells (BV2) or primary microglia (Mic) cultures that were exposed to the indicated $MnCl_2$ concentrations for 6 h. The β -tubulin was used as loading control. (b) Quantification of the SPCA1 upper (non-striped bars) and lower (striped bars) bands normalized to the loading control. They were normalized to the SPCA1 lower band in the absence of Mn^{2+} (value of 1.0 arbitrary units) in both BV2 and primary microglial cells. (c) SPCA-dependent Ca^{2+} -ATPase activity from membrane vesicles of BV2 control cells measured in the presence of the indicated $MnCl_2$ concentrations. 100% SPCA activity corresponds to $0.065 \pm 0.01 \mu\text{mol min}^{-1} \text{mg}^{-1}$. (d) Cell viability after exposure to 2.5 mM $MnCl_2$ in control, SPCA1-silenced and SPCA1-overexpressed BV2 cells. Data represent mean \pm SEM of three experiments, performed in duplicates. *, $p < .05$ compared with control cells treated with $MnCl_2$.

transporters of the ER (SERCA2b) (Morales-Ropero et al., 2021) or Golgi (SPCA1, this work). We failed to detect SPCA2 with specific antibodies (data not shown), which is in line with gene expression databases highlighting an almost complete absence of *Atp2c2* transcripts in mouse microglia (Saunders et al., 2018), suggesting that SPCA1 represents the primary isoform in microglia.

Two closely spaced protein bands around 100 kDa were recognized by Western blot with the anti-SPCA1 antibody in microglia, while only the lower protein band was observed in mouse brain extracts. Similarly, only the lower band was observed in cultured murine neurons and astrocytes protein extracts (Sepulveda, Wuytack, & Mata, 2012). This protein might correspond to the SPCA1a variant in humans, the major variant in brain. The other human SPCA1 variants b, c, d, e, and f obtained by alternative splicing have not been identified in mouse (Micaroni & Malquori, 2013; Sepulveda et al., 2008). Therefore, the upper band may involve post-translational modifications of SPCA1 that requires further investigation. Nevertheless, SPCA1 double bands have also been observed in mouse cerebellum, that were upregulated during development (Sepulveda et al., 2008), or in mouse parotid and thyroid glands (Sepulveda, Wuytack, & Mata, 2012), indicating a modulated expression of SPCA1 in certain tissues or cell types according to specific

requirements. On the other hand, the perinuclear location of SPCA1 at the Golgi apparatus in microglia matches with the one observed in other brain cell types (Sepulveda et al., 2008). Interestingly, LPS-stimulated microglia showed a dispersion of Golgi stacks that can be associated with cellular reorganization occurring during morphological changes triggered by LPS in these cells. Indeed, SPCA1 in the Golgi Ca^{2+} homeostasis is required for a directed flow of protein and membrane traffic in cells (Sepulveda et al., 2009).

To analyze the role of SPCA1 in microglia, we modulated SPCA1 expression by silencing and overexpression. Although we did not observe effects on microglial viability, probably because compensatory effects of other Ca^{2+} homeostatic players, cells displayed a shift towards an amoeboid morphology, a change in cell area and altered phagocytic capacity. This was especially evident when overexpressed SPCA1 appeared in fragmented Golgi stacks throughout the cytoplasm. SPCA1 overexpression in other cell types was also related with Golgi stress, and it has been associated to a store-independent Ca^{2+} entry by coupling SPCA1 and Orai1, inducing cytosolic Ca^{2+} influx (Smaardijk et al., 2018). Alterations in intraluminal and cytosolic Ca^{2+} levels causes cytoskeletal disruptions, defects in maturation, trafficking and sorting of proteins, or modulation of Golgi structural problems, contributing to Golgi fragmentation (Joshi et al., 2015).

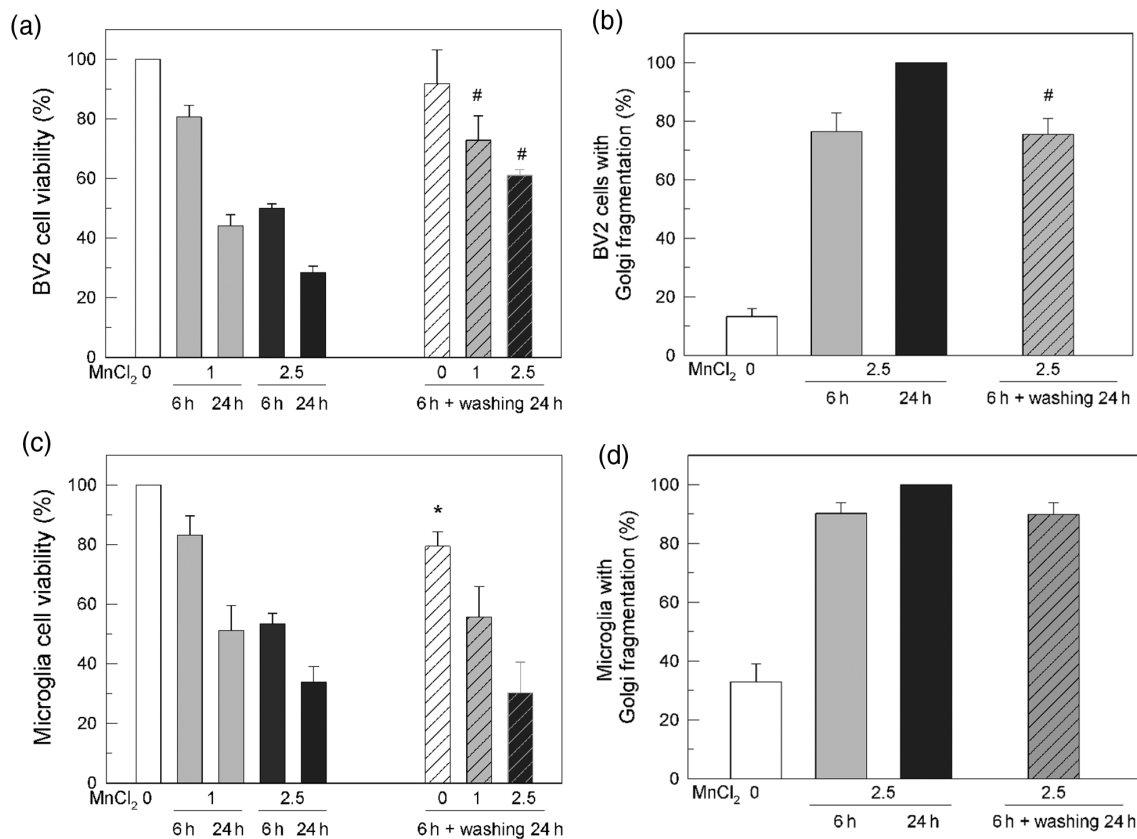


FIGURE 6 Cell survival and Golgi integrity after washing out Mn²⁺. Cell viability and Golgi fragmentation were determined after exposure of Mn²⁺ to BV2 cells (a, b) and primary microglia (c, d) to the indicated MnCl₂ concentrations for 6 or 24 h. Alternatively, after 6 h-treatment, the medium was changed to medium from untreated cultures and incubated for additional 24 h. Data represent mean ± SEM of three experiments, performed in triplicates. To quantify Golgi fragmentation, we analyzed at least 50 cells per condition in each experiment. *p* < .05 compared with the same MnCl₂ concentration at 6 h (*) or 24 h (#) without washing.

Golgi fragmentation involves unlinking the stacks in the ribbon, which occurs reversibly in physiological conditions such as mitosis or migration, but there are increasing evidences of its association to pathological conditions. Golgi fragmentation emerges as an early histological sign of cellular damage prior to apoptosis in multiple disorders including neurodegenerative diseases (Gonatas et al., 2006; Makhoul et al., 2019). Here, we found Golgi fragmentation not only after SPCA1 overexpression but also after Mn²⁺ exposure in cultured microglia. While Mn²⁺ is an essential element, in excess it can be severely toxic, especially in the brain. Occupational or environmental overexposure to Mn²⁺ leads to manganism, a Parkinson's disease-like syndrome that causes serious neurological and behavioral symptoms, with high prevalence in workers such as welders, miners, or smelters (Racette et al., 2017). Mn²⁺ intoxication reaches the brain, where it is taken up by cells through the plasma membrane mainly by divalent metal channels, increasing Mn²⁺ cytosolic levels that are afterwards accumulated in Golgi cisternae (Carmona et al., 2010). In this context, the Golgi apparatus may represent a primary Mn²⁺ storage site that relies on the Mn²⁺ transport capacity of SPCA to reduce excess cytosolic Mn²⁺ for further elimination via the secretory pathway. In fact, there is a correlation between Mn²⁺ depositions in brain monitored by Mn²⁺-enhanced magnetic resonance imaging and SPCA1-enriched

areas (Sepulveda, Dresselaers, et al., 2012). However, Mn²⁺ can inhibit the Ca²⁺-transport activity of SPCA, since the transport of Mn²⁺ and Ca²⁺ in SPCA is mutually exclusive because both ions have the same ion-binding site for transport (Van Baelen et al., 2001). Thus, Mn²⁺ toxicity may impair Ca²⁺ homeostasis possibly translating into the disruption of Ca²⁺ gradients and membrane dynamics along the Golgi ribbon structure and secretory pathway. The effect of Mn²⁺ on Golgi fragmentation has also been observed in neurons and astrocytes in culture (Sepulveda, Wuytack, & Mata, 2012) and other cell types (Towler et al., 2000).

Furthermore, high Mn²⁺ overexposure reduced cell viability of microglia, although with IC₅₀ values higher than those obtained in astrocytes or neurons (Sepulveda, Wuytack, & Mata, 2012). This could be related with the neuroprotective and possible detoxifying role of microglia compared with other cell types in brain, although on the other hand, Mn²⁺-exposed microglia enhanced the expression of pro-inflammatory cytokines in astrocytes (Kirkley et al., 2017) that contribute to degeneration and cell death.

Previous *in vitro* studies have shown that Mn²⁺ withdrawal improved survival of neurons and astrocytes and allowed partial recovery of the Golgi integrity (Sepulveda, Wuytack, & Mata, 2012), although this is less evident in microglia. Accordingly, the cessation of

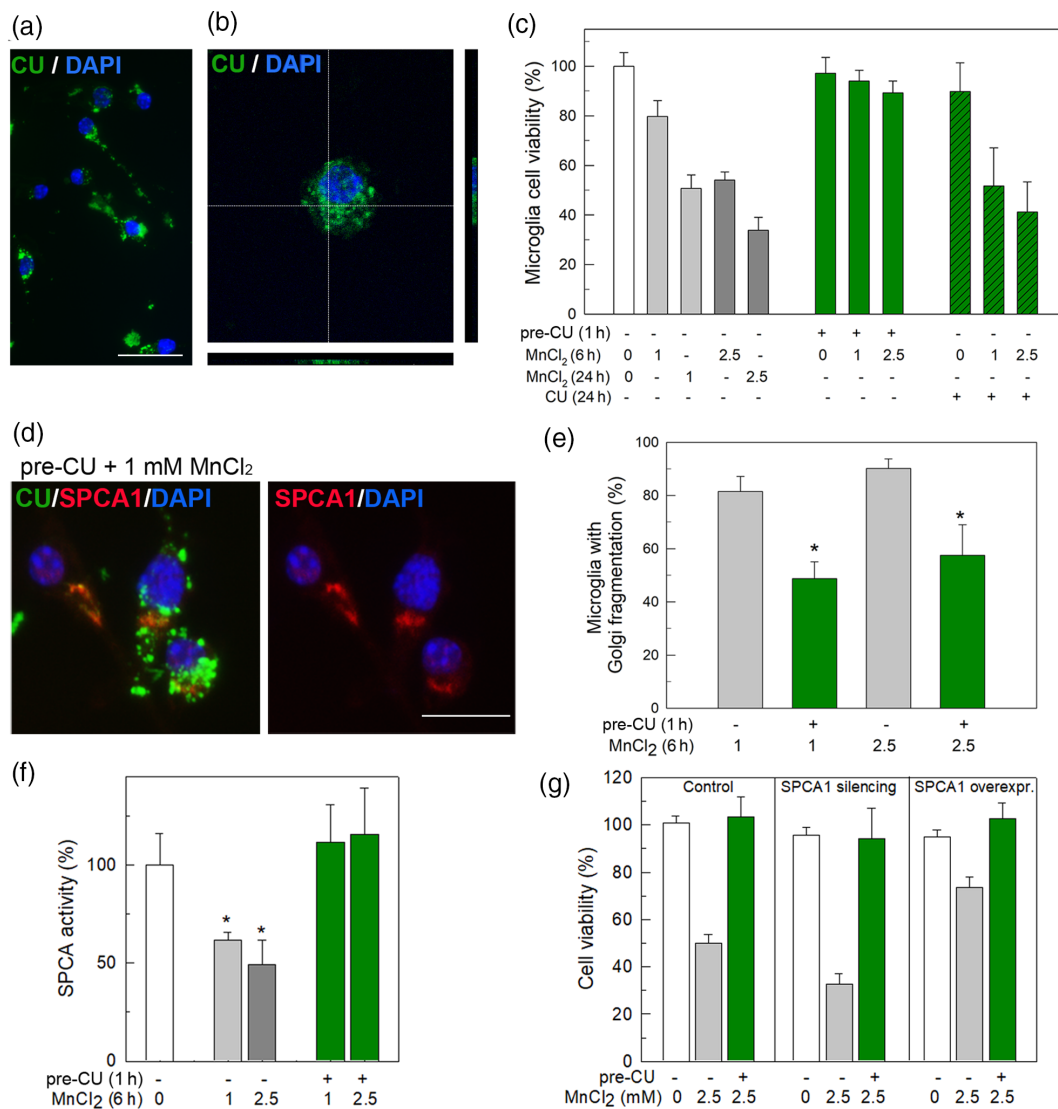


FIGURE 7 Effect of curcumin on Golgi fragmentation and SPCA1 activity in Mn^{2+} exposed microglia. (a) Curcumin uptake (CU, green) in primary microglia was followed by fluorescence microscopy. DAPI staining (blue) was used to visualize nuclei. (b) An orthogonal projection obtained by confocal microscopy showed that curcumin was inside the cell. (c) Determination of cell viability on primary cultures of microglia treated with $10 \mu M$ curcumin before or after Mn^{2+} exposure at the indicated concentrations and time points. (d) SPCA1 immunoreaction (red) on primary microglia pre-treated 1 h with $10 \mu M$ curcumin (green) and further exposed to 1 mM $MnCl_2$ for 6 h. The Golgi apparatus remains unfragmented. (e) Quantification of cells with Golgi fragmentation with or without curcumin pretreatment at 1 or 2.5 mM $MnCl_2$, showing a significant reduction in conditions with curcumin pretreatment. (f) Measurements of SPCA Ca^{2+} -ATPase activity that was preserved from Mn^{2+} inhibition when cells were pretreated with curcumin. (g) Effect of curcumin pretreatment on cell viability of control, SPCA1-silenced and SPCA1-overexpressed BV2 cells exposed to 2.5 mM $MnCl_2$. Data represent mean \pm SEM of three experiments, performed in triplicates. To quantify Golgi fragmentation, we analyzed at least 50 cells per condition in each experiment. *, $p < .05$ compared to controls. Scale bars: 30 μm (a), 20 μm (d). SPCA1, secretory pathway Ca^{2+}/Mn^{2+} -transport ATPase isoform 1.

Mn^{2+} overexposure has been reported to improve cognitive and motor problems and to reduce Mn^{2+} accumulation in the brain in animal models (Sepulveda, Dresselaers, et al., 2012) and patients (Ono et al., 2002); however, they did not reach full recovery.

In search of compounds to alleviate the manganese disorder, curcumin has been proposed as a therapeutic tool for Mn^{2+} -induced microglial cell death (Park & Chun, 2017). Curcumin is a polyphenol molecule in the rhizome of *Curcuma longa* (Zingiberaceae), which has traditionally been used in Asian countries for medicine or cooking (Pulido-Moran et al., 2016). This compound presents antioxidant, anti-

inflammatory, and immunoregulatory properties (Hamzehzadeh et al., 2018; Shakeri et al., 2019). It has been reported that curcumin is able to cross the blood-brain barrier and acts as a potent modulator of the microglia phenotype (Ghasemi et al., 2019; Tsai et al., 2011). Accumulating evidences have demonstrated how curcumin is able to change the microglial transcriptome, to inhibit the release of pro-inflammatory cytokines and ROS production, or to stimulate phagocytic functions (Karlstetter et al., 2011; Ono et al., 2004; Parada et al., 2015). However, in our work, curcumin did not induce a full recovery when it was used as posttreatment after Mn^{2+} toxicity.

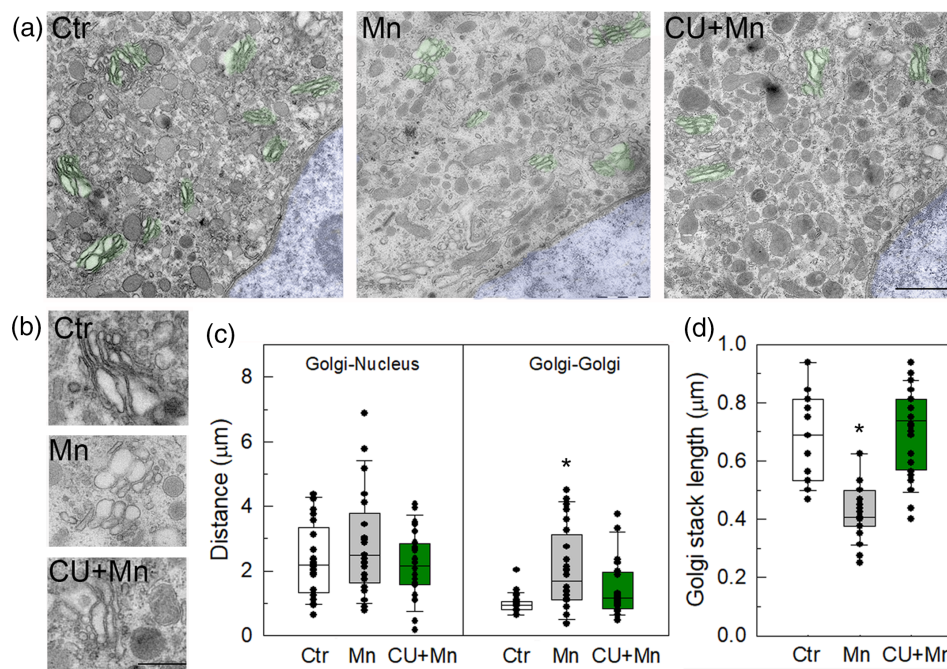


FIGURE 8 Analysis of the Golgi apparatus in primary microglia by transmission electron microscopy. (a) Control microglia (Ctr) shows Golgi stacks (pseudo-colored in green) in close proximity to the nucleus (in blue) while dispersed Golgi mini-stacks were observed after 6 h of 1 mM MnCl_2 (Mn) exposure to microglia. Curcumin pretreatment for 1 h before Mn^{2+} exposure prevented Golgi fragmentation (CU + Mn). (b) Magnification of Golgi stacks in the three experimental conditions. (c, d) Box plots of distances from Golgi stacks to the nucleus, between Golgi stacks (c) and the Golgi cisternae lengths (d) in the three experimental conditions. Data represent mean \pm SEM. At least five cells per condition were analyzed, counting at least seven Golgi stacks per cell. *, $p < .05$ compared with controls. Scale bars: 1 μm (a), 0.5 μm (b).

Our results present curcumin as a potential protective agent against microglial Mn^{2+} toxicity. Thus, curcumin may possibly be considered as a preventive and protective compound to people exposed to environments with high Mn^{2+} levels.

Recent epidemiologic studies have documented that Mn^{2+} over-exposure increases the risk and prevalence of Alzheimer's disease and other dementias (Bakulski et al., 2020). As mentioned above, part of the first episodes of these diseases consists in Ca^{2+} dyshomeostasis, early Golgi fragmentation, and inability to correctly engulf toxic particles (Tillemont & Papadopoulos, 2014). Since SPCA1 is involved in these processes, understanding the impact of this secretory pathway $\text{Ca}^{2+}/\text{Mn}^{2+}$ transporter in microglia will be important towards developing therapeutic strategies.

AUTHOR CONTRIBUTIONS

JN and MRS conceived the study. MRS coordinated and designed experiments and provided funding. AMB-C, AB-G, VEN, FAM-J, DM-O and MRS performed research. AMB-C, MB, DM-O, MAC, JLM-T, JN, and MRS analyzed data. PV contributed antibodies and discussed data. VEN, PV and MRS wrote the manuscript. The final version of the manuscript was revised and approved by all authors.

ACKNOWLEDGMENTS

A.B.-C. received a postgraduate scholarship provided by Ministry of Education, Culture and Sports, Spain. We thank Drs J.D. Bueno,

M.J. Martínez and D. Porcel for their valuable advice at the Scientific Instrumentation Center (UGR) and the Dept. of Biochemistry and Molecular Biology I (UGR) for kindly allowing us to use some of their devices. We also thank J.M. Morales-Ropero for his input in the beginning of the project. This work was funded by grants A1-CTS-324-UGR18 from FEDER-Junta de Andalucía and PP2022.PP.29 from UGR Research Program, Spain.

DATA AVAILABILITY STATEMENT

The data that support the findings of this study are available from the corresponding author upon reasonable request.

ORCID

Aysha M. Bhojwani-Cabrera <https://orcid.org/0009-0006-3290-9173>

Alicia Bautista-García <https://orcid.org/0009-0005-9585-0247>

Veronika E. Neubrand <https://orcid.org/0000-0002-3793-8487>

Francisco A. Membrive-Jiménez <https://orcid.org/0009-0005-6669-744X>

Mattia Bramini <https://orcid.org/0000-0002-0381-9391>

David Martin-Oliva <https://orcid.org/0000-0002-8095-5442>

Miguel A. Cuadros <https://orcid.org/0000-0003-4259-1649>

José Luis Marín-Teva <https://orcid.org/0000-0002-5829-4502>

Julio Navascués <https://orcid.org/0000-0003-2958-2705>

Peter Vangheluwe <https://orcid.org/0000-0002-7822-2944>

M. Rosario Sepúlveda <https://orcid.org/0000-0002-2375-5866>

REFERENCES

- Alawieyah Syed Mortadza, S., Sim, J. A., Neubrand, V. E., & Jiang, L. H. (2018). A critical role of TRPM2 channel in Abeta(42)-induced microglial activation and generation of tumor necrosis factor-alpha. *Glia*, 66(3), 562–575. <https://doi.org/10.1002/glia.23265>
- Aschner, M., Erikson, K. M., Herrero Hernandez, E., & Tjalkens, R. (2009). Manganese and its role in Parkinson's disease: From transport to neuropathology. *Neuromolecular Medicine*, 11(4), 252–266. <https://doi.org/10.1007/s12017-009-8083-0>
- Avila, D. S., Puntel, R. L., & Aschner, M. (2013). Manganese in health and disease. *Metal Ions in Life Sciences*, 13, 199–227. https://doi.org/10.1007/978-94-007-7500-8_7
- Bakulski, K. M., Seo, Y. A., Hickman, R. C., Brandt, D., Vadari, H. S., Hu, H., & Park, S. K. (2020). Heavy metals exposure and Alzheimer's disease and related dementias. *Journal of Alzheimer's Disease*, 76(4), 1215–1242. <https://doi.org/10.3233/JAD-200282>
- Benedetto, A., Au, C., & Aschner, M. (2009). Manganese-induced dopaminergic neurodegeneration: Insights into mechanisms and genetics shared with Parkinson's disease. *Chemical Reviews*, 109(10), 4862–4884. <https://doi.org/10.1021/cr800536y>
- Carmona, A., Deves, G., Roudeau, S., Cloetens, P., Bohic, S., & Ortega, R. (2010). Manganese accumulates within Golgi apparatus in dopaminergic cells as revealed by synchrotron X-ray fluorescence nanoimaging. *ACS Chemical Neuroscience*, 1(3), 194–203. <https://doi.org/10.1021/cn900021z>
- Chen, J., Sitsel, A., Benoy, V., Sepulveda, M. R., & Vangheluwe, P. (2020). Primary active Ca(2+) transport systems in health and disease. *Cold Spring Harbor Perspectives in Biology*, 12(2), a035113. <https://doi.org/10.1101/cshperspect.a035113>
- Feng, M. Y., & Rao, R. (2013). New insights into store-independent Ca(2+) entry: Secretory pathway calcium ATPase 2 in normal physiology and cancer. *International Journal of Oral Science*, 5(2), 71–74. <https://doi.org/10.1038/ijos.2013.23>
- Friedman, B. A., Srinivasan, K., Ayalon, G., Meilandt, W. J., Lin, H., Huntley, M. A., Cao, Y., Lee, S.-H., Haddick, P. C. G., Ngu, H., Modrusan, Z., Larson, J. L., Kaminker, J. S., van der Brug, M. P., & Hansen, D. V. (2018). Diverse brain myeloid expression profiles reveal distinct microglial activation states and aspects of Alzheimer's disease not evident in mouse models. *Cell Reports*, 22(3), 832–847. <https://doi.org/10.1016/j.celrep.2017.12.066>
- Ghasemi, F., Bagheri, H., Barreto, G. E., Read, M. I., & Sahebkar, A. (2019). Effects of curcumin on microglial cells. *Neurotoxicity Research*, 36(1), 12–26. <https://doi.org/10.1007/s12640-019-00030-0>
- Gonatas, N. K., Stieber, A., & Gonatas, J. O. (2006). Fragmentation of the Golgi apparatus in neurodegenerative diseases and cell death. *Journal of the Neurological Sciences*, 246(1–2), 21–30. <https://doi.org/10.1016/j.jns.2006.01.019>
- Hamzehzadeh, L., Atkin, S. L., Majeed, M., Butler, A. E., & Sahebkar, A. (2018). The versatile role of curcumin in cancer prevention and treatment: A focus on PI3K/AKT pathway. *Journal of Cellular Physiology*, 233(10), 6530–6537. <https://doi.org/10.1002/jcp.26620>
- Henn, A., Lund, S., Hedtjarn, M., Schratzenholz, A., Porzgen, P., & Leist, M. (2009). The suitability of BV2 cells as alternative model system for primary microglia cultures or for animal experiments examining brain inflammation. *ALTEX*, 26(2), 83–94. Retrieved from http://www.ncbi.nlm.nih.gov/entrez/query.fcgi?cmd=Retrieve&db=PubMed&dopt=Citation&list_uids=19565166
- Hoffmann, A., Kann, O., Ohlemeyer, C., Hanisch, U. K., & Kettenmann, H. (2003). Elevation of basal intracellular calcium as a central element in the activation of brain macrophages (microglia): Suppression of receptor-evoked calcium signaling and control of release function. *The Journal of Neuroscience*, 23(11), 4410–4419. <https://doi.org/10.1523/JNEUROSCI.23-11-04410.2003>
- Joshi, G., Bekier, M. E., 2nd, & Wang, Y. (2015). Golgi fragmentation in Alzheimer's disease. *Frontiers in Neuroscience*, 9, 340. <https://doi.org/10.3389/fnins.2015.00340>
- Karlstetter, M., Lippe, E., Walczak, Y., Moehle, C., Aslanidis, A., Mirza, M., & Langmann, T. (2011). Curcumin is a potent modulator of microglial gene expression and migration. *Journal of Neuroinflammation*, 8, 125. <https://doi.org/10.1186/1742-2094-8-125>
- Kirkley, K. S., Popichak, K. A., Afzali, M. F., Legare, M. E., & Tjalkens, R. B. (2017). Microglia amplify inflammatory activation of astrocytes in manganese neurotoxicity. *Journal of Neuroinflammation*, 14(1), 99. <https://doi.org/10.1186/s12974-017-0871-0>
- Makhoul, C., Gosavi, P., & Gleeson, P. A. (2019). Golgi dynamics: The morphology of the mammalian Golgi apparatus in health and disease. *Frontiers in Cell and Development Biology*, 7, 112. <https://doi.org/10.3389/fcell.2019.00112>
- Micaroni, M., & Malquori, L. (2013). Overlapping ATP2C1 and ASTE1 genes in human genome: Implications for SPCA1 expression? *International Journal of Molecular Sciences*, 14(1), 674–683. <https://doi.org/10.3390/ijms14010674>
- Morales-Roperio, J. M., Arroyo-Urea, S., Neubrand, V. E., Martin-Oliva, D., Marin-Teva, J. L., Cuadros, M. A., Vangheluwe, P., Navascués, J., Mata, A. M., & Sepulveda, M. R. (2021). The endoplasmic reticulum Ca(2+) -ATPase SERCA2b is upregulated in activated microglia and its inhibition causes opposite effects on migration and phagocytosis. *Glia*, 69(4), 842–857. <https://doi.org/10.1002/glia.23931>
- Neubrand, V. E., Forte-Lago, I., Caro, M., & Delgado, M. (2018). The atypical RhoGTPase RhoE/Rnd3 is a key molecule to acquire a neuroprotective phenotype in microglia. *Journal of Neuroinflammation*, 15(1), 343. <https://doi.org/10.1186/s12974-018-1386-z>
- Ono, K., Hasegawa, K., Naiki, H., & Yamada, M. (2004). Curcumin has potent anti-amyloidogenic effects for Alzheimer's beta-amyloid fibrils in vitro. *Journal of Neuroscience Research*, 75(6), 742–750. <https://doi.org/10.1002/jnr.20025>
- Ono, K., Komai, K., & Yamada, M. (2002). Myoclonic involuntary movement associated with chronic manganese poisoning. *Journal of the Neurological Sciences*, 199(1–2), 93–96. [https://doi.org/10.1016/s0022-510x\(02\)00111-9](https://doi.org/10.1016/s0022-510x(02)00111-9)
- Parada, E., Buendia, I., Navarro, E., Avendano, C., Egea, J., & Lopez, M. G. (2015). Microglial HO-1 induction by curcumin provides antioxidant, anti-neuroinflammatory, and glioprotective effects. *Molecular Nutrition & Food Research*, 59(9), 1690–1700. <https://doi.org/10.1002/mnfr.201500279>
- Park, E., & Chun, H. S. (2017). Protective effects of curcumin on manganese-induced BV-2 microglial cell death. *Biological & Pharmaceutical Bulletin*, 40(8), 1275–1281. <https://doi.org/10.1248/bpb.b17-00160>
- Pulido-Moran, M., Moreno-Fernandez, J., Ramirez-Tortosa, C., & Ramirez-Tortosa, M. (2016). Curcumin and health. *Molecules*, 21(3), 264. <https://doi.org/10.3390/molecules21030264>
- Racette, B. A., Aschner, M., Guilarte, T. R., Dydak, U., Criswell, S. R., & Zheng, W. (2012). Pathophysiology of manganese-associated neurotoxicity. *Neurotoxicology*, 33(4), 881–886. <https://doi.org/10.1016/j.neuro.2011.12.010>
- Racette, B. A., Searles Nielsen, S., Criswell, S. R., Sheppard, L., Seixas, N., Warden, M. N., & Checkoway, H. (2017). Dose-dependent progression of parkinsonism in manganese-exposed welders. *Neurology*, 88(4), 344–351. <https://doi.org/10.1212/WNL.0000000000003533>
- Saunders, A., Macosko, E. Z., Wysoker, A., Goldman, M., Krienen, F. M., de Rivera, H., Bien, E., Baum, M., Bortolin, L., Wang, S., Goeva, A., Nemes, J., Kamitaki, N., Brumbaugh, S., Kulp, D., & McCarroll, S. A. (2018). Molecular diversity and specializations among the cells of the adult mouse brain. *Cell*, 174(4), 1015–1030 e1016. <https://doi.org/10.1016/j.cell.2018.07.028>
- Sepulveda, M. R., Dresselaers, T., Vangheluwe, P., Everaerts, W., Himmelreich, U., Mata, A. M., & Wuytack, F. (2012). Evaluation of manganese uptake and toxicity in mouse brain during continuous MnCl2 administration using osmotic pumps. *Contrast Media & Molecular Imaging*, 7(4), 426–434. <https://doi.org/10.1002/cmml.1469>



- Sepulveda, M. R., Hidalgo-Sanchez, M., & Mata, A. M. (2005). A developmental profile of the levels of calcium pumps in chick cerebellum. *Journal of Neurochemistry*, 95(3), 673–683. <https://doi.org/10.1111/j.1471-4159.2005.03401.x>
- Sepulveda, M. R., Marcos, D., Berrocal, M., Raeymaekers, L., Mata, A. M., & Wuytack, F. (2008). Activity and localization of the secretory pathway Ca²⁺-ATPase isoform 1 (SPCA1) in different areas of the mouse brain during postnatal development. *Molecular and Cellular Neurosciences*, 38(4), 461–473. <https://doi.org/10.1016/j.mcn.2008.02.012>
- Sepulveda, M. R., Vanoevelen, J., Raeymaekers, L., Mata, A. M., & Wuytack, F. (2009). Silencing the SPCA1 (secretory pathway Ca²⁺-ATPase isoform 1) impairs Ca²⁺ homeostasis in the Golgi and disturbs neural polarity. *The Journal of Neuroscience*, 29(39), 12174–12182. <https://doi.org/10.1523/JNEUROSCI.2014-09.2009>
- Sepulveda, M. R., Wuytack, F., & Mata, A. M. (2012). High levels of Mn²⁺ inhibit secretory pathway Ca²⁺/Mn²⁺-ATPase (SPCA) activity and cause Golgi fragmentation in neurons and glia. *Journal of Neurochemistry*, 123(5), 824–836. <https://doi.org/10.1111/j.1471-4159.2012.07888.x>
- Shakeri, A., Panahi, Y., Johnston, T. P., & Sahebkar, A. (2019). Biological properties of metal complexes of curcumin. *BioFactors*, 45(3), 304–317. <https://doi.org/10.1002/biof.1504>
- Sierra, A., Paolicelli, R. C., & Kettenmann, H. (2019). Cien Anos de microglia: Milestones in a century of microglial research. *Trends in Neurosciences*, 42(11), 778–792. <https://doi.org/10.1016/j.tins.2019.09.004>
- Smaardijk, S., Chen, J., Kerselaers, S., Voets, T., Eggermont, J., & Vangheluwe, P. (2018). Store-independent coupling between the secretory pathway Ca(2+) transport ATPase SPCA1 and Orai1 in Golgi stress and Hailey-Hailey disease. *Biochim Biophys Acta Mol Cell Res*, 1865(6), 855–862. <https://doi.org/10.1016/j.bbamcr.2018.03.007>
- Tang, Y., & Le, W. (2016). Differential roles of M1 and M2 microglia in neurodegenerative diseases. *Molecular Neurobiology*, 53(2), 1181–1194. <https://doi.org/10.1007/s12035-014-9070-5>
- Tillement, J. P., & Papadopoulos, V. (2014). Subcellular injuries in Alzheimer's disease. *CNS & Neurological Disorders Drug Targets*, 13(4), 593–605. <https://doi.org/10.2174/18715273113126660197>
- Ton, V. K., Mandal, D., Vahadji, C., & Rao, R. (2002). Functional expression in yeast of the human secretory pathway Ca(2+), Mn(2+)-ATPase defective in Hailey-Hailey disease. *The Journal of Biological Chemistry*, 277(8), 6422–6427. <https://doi.org/10.1074/jbc.M110612200>
- Towler, M. C., Prescott, A. R., James, J., Lucocq, J. M., & Ponnambalam, S. (2000). The manganese cation disrupts membrane dynamics along the secretory pathway. *Experimental Cell Research*, 259(1), 167–179. <https://doi.org/10.1006/excr.2000.4958>
- Tsai, Y. M., Chien, C. F., Lin, L. C., & Tsai, T. H. (2011). Curcumin and its nano-formulation: The kinetics of tissue distribution and blood-brain barrier penetration. *International Journal of Pharmaceutics*, 416(1), 331–338. <https://doi.org/10.1016/j.ijpharm.2011.06.030>
- Van Baelen, K., Vanoevelen, J., Missiaen, L., Raeymaekers, L., & Wuytack, F. (2001). The Golgi PMR1 P-type ATPase of *Caenorhabditis elegans*. Identification of the gene and demonstration of calcium and manganese transport. *The Journal of Biological Chemistry*, 276(14), 10683–10691. <https://doi.org/10.1074/jbc.M010553200>
- Vanoevelen, J., Dode, L., Van Baelen, K., Fairclough, R. J., Missiaen, L., Raeymaekers, L., & Wuytack, F. (2005). The secretory pathway Ca²⁺/Mn²⁺-ATPase 2 is a Golgi-localized pump with high affinity for Ca²⁺ ions. *The Journal of Biological Chemistry*, 280(24), 22800–22808. <https://doi.org/10.1074/jbc.M501026200>
- Wolf, S. A., Boddeke, H. W., & Kettenmann, H. (2017). Microglia in physiology and disease. *Annual Review of Physiology*, 79, 619–643. <https://doi.org/10.1146/annurev-physiol-022516-034406>

SUPPORTING INFORMATION

Additional supporting information can be found online in the Supporting Information section at the end of this article.

How to cite this article: Bhojwani-Cabrera, A. M., Bautista-García, A., Neubrand, V. E., Membrive-Jiménez, F. A., Bramini, M., Martin-Oliva, D., Cuadros, M. A., Marín-Teva, J. L., Navascués, J., Vangheluwe, P., & Sepúlveda, M. R. (2024). Upregulation of the secretory pathway Ca²⁺/Mn²⁺-ATPase isoform 1 in LPS-stimulated microglia and its involvement in Mn²⁺-induced Golgi fragmentation. *Glia*, 1–14. <https://doi.org/10.1002/glia.24528>